Physics of the Earth and Planetary Interiors 178 (2010) 162–175

Contents lists available at ScienceDirect

Physics of the Earth and Planetary Interiors

journal homepage: www.elsevier.com/locate/pepi

Shear-driven upwelling induced by lateral viscosity variations and asthenospheric shear: A mechanism for intraplate volcanism

Clinton P. Conrad[a,*], Benjun Wu[b], Eugene I. Smith[c], Todd A. Bianco[a], Ashley Tibbetts[c]

[a] Department of Geology and Geophysics, SOEST, University of Hawaii, Honolulu HI 96822, United States
[b] Department of Earth and Planetary Sciences, Johns Hopkins University, Baltimore MD 21218, United States
[c] Department of Geoscience, University of Nevada at Las Vegas, Las Vegas NV 89154, United States

ARTICLE INFO

Article history:
Received 24 March 2009
Received in revised form 6 October 2009
Accepted 6 October 2009

Keywords:
Intraplate volcanism
Asthenospheric upwelling
Upper Mantle Flow
Plate motions
Viscous shear
Viscosity heterogeneity
Melting instability

ABSTRACT

Volcanism occurring away from ridges and subduction zones does not have an obvious plate tectonic explanation, but instead must arise from sub-lithospheric processes that generate upwelling flow and decompression melting. Several convective processes, such as mantle plumes, convective instability, edge-driven convection, and Richter rolls, produce upwelling via the action of gravity on density heterogeneities in the mantle. Here we investigate an alternative mechanism, the shear-driven upwelling (SDU), which instead generates upwelling solely through the action of asthenospheric shear flow on viscosity heterogeneity. Using a numerical flow model, we examine the effect of viscosity heterogeneity on viscous shear flow induced within an asthenospheric layer. We demonstrate that for certain geometries and viscosity ratios, circulatory flow develops within a "cavity" or "step" embedded into the lithospheric base, or within a low-viscosity "pocket" embedded within the asthenospheric layer. For asthenosphere shearing at 5 cm/yr, we estimate that SDU can produce upwelling rates of up to ~0.2 cm/yr within a continental rift, ~0.5 cm/yr along the vertical edge of a craton, or ~1.0 cm/yr within a "pocket" of low-viscosity asthenosphere. In the last case, the pocket must feature an aspect ratio of more than 5, occupy ~20–60% of the asthenosphere's thickness, and be at least 100 times less viscous than the surrounding asthenosphere. Such viscosity heterogeneity may be associated with thermal, chemical, melting, volatile, or grain-size anomalies, and is consistent with tomographic constraints on asthenospheric variability. We estimate that SDU may generate up to 2.5 km/Myr of melt that is potentially eruptible as surface volcanism; this is faster than eruption rates observed at some locations of continental basaltic volcanism. We conclude that SDU could provide an explanation for intraplate volcanism occurring above rapidly shearing asthenosphere, for example in the Basin and Range region of North America.

1. Introduction

Most of the volcanism around the globe occurs at subduction zones and mid-ocean ridges, and is well-explained by the theory of plate tectonics. Volcanism that occurs away from plate boundaries, however, is less easily explained, but has often been attributed to hot plumes that rise from deep within the mantle (Morgan, 1971). Such plumes are a natural consequence of mantle convection and provide an explanation for the numerous linear chains of volcanoes around the globe (e.g., Richards et al., 1989). Recently, however, the plume explanation for intraplate volcanism has been challenged (e.g., Foulger and Natland, 2003), and alternative explanations such as lithospheric cracking have been proposed (e.g., Anderson, 2000). Recent studies have suggested that relatively few (less than 10) volcanic chains are caused by deep mantle plumes (e.g. Courtillot et al., 2003), out of upwards of 30–40 hotspot tracks that have previously been attributed to plumes (e.g., Sleep, 1990; Steinberger, 2000). Thus, regardless of whether the major hotspots (e.g., Iceland, Hawaii, Louisville) are plume-generated, an alternative explanation is needed to explain intraplate volcanism not fed by plumes.

Furthermore, several other intraplate volcanic features, such as seamounts that pervade the Pacific basin (Hillier and Watts, 2007), are not associated with classic hotspot tracks (Clouard and Bonneville, 2001). Instead most Pacific seamounts were emplaced during the Cretaceous along with the large Pacific oceanic plateaus (Wessel, 1997). More recently, the southwestern US has become dotted by mid-Miocene to contemporary basaltic volcanic fields, such as the Death Valley-Lunar Crater belt, the Saint George volcanic Field, and the Jemez lineament. These features do not resemble plume-induced volcanism in terms of their temporal and spatial patterns (Smith et al., 2002; Smith and Keenan, 2005), associated uplift (Parsons et al., 1994), or volumetric output (Bradshaw et al., 1993; Hawkesworth et al., 1995). Other examples of non-plume intraplate volcanism, such as in the Harrat Ash Shaam field

* Corresponding author. Tel.: +1 808 956 6649; fax: +1 808 956 5154.
E-mail address: clintc@hawaii.edu (C.P. Conrad).

0031-9201/$ – see front matter © 2009 Elsevier B.V. All rights reserved.
doi:10.1016/j.pepi.2009.10.001

in the Middle East (e.g., Shaw et al., 2003), and the Changbai volcano in Northeast Asia (Lei and Zhao, 2005), have been noted in several locations around the world.

Without a source of excess heat coming from the deep mantle, most alternative explanations for intraplate volcanism invoke some source of regional asthenospheric upwelling that induces decompression melting. This melting may be augmented by "melting instabilities" that involve positive feedback between decompression melting and the subsequent upwelling caused by the presence of this melt (Raddick et al., 2002; Hernlund et al., 2008a,b). This feedback can result in an episode of volcanism above asthenosphere near its melting temperature. Thus, the search for a non-plume source of intraplate volcanism generally involves a search for mechanisms that can initiate upwelling flow within fertile asthenosphere that is already near its solidus. Several upwelling mechanisms have been proposed. First, the presence of extension generates passive upwelling flow (e.g., McKenzie and Bickle, 1988), but this flow should be extremely slow unless it becomes localized in some way. In addition, numerical models show that melting instabilities may be inhibited or delayed by the presence of active lithospheric extension (Hernlund et al., 2008b). Alternatively, the temperature differential between the lithosphere and asthenosphere sets up an inverted density structure that can lead to persistent steady-state thermal convection in the asthenosphere (e.g., Haxby and Weissel, 1986; van Hunen and Zhong, 2006; Ballmer et al., 2007) or occasional "drips" of dense lithosphere sinking into the upper mantle (e.g., Le Pourhiet et al., 2006). Both convection and "dripping" involve asthenospheric upwelling that can lead to volcanism, and may be enhanced by viscosity heterogeneity or lithospheric deformation (e.g., Conrad, 2000). Finally, small-scale convection in the asthenosphere may be enhanced near the edges of cratons or other sharp gradients in lithospheric thickness because the associated lateral temperature gradients can produce an "edge-driven" convective circulation in the asthenosphere (e.g., King and Anderson, 1998) that can lead to volcanism (King and Ritsema, 2000).

The density inversion between the lithosphere and asthenosphere is not the only energy source that can drive small-scale asthenospheric circulation and upwelling. For example, the asthenosphere accommodates up to a few cm/yr of relative motion between the lithospheric plates and the convecting mantle via a shearing deformation that can be detected by observations of seismic anisotropy (e.g., Silver and Holt, 2002; Conrad et al., 2007). When asthenospheric shear occurs simultaneously with small-scale convection, the density heterogeneity produced by convection becomes elongated into roll-like circulatory structures known as "Richter Rolls" (e.g., Richter and Parsons, 1975; Korenaga and Jordan, 2003). Less well-studied, however, is the response of a shear flow to viscosity heterogeneity, either within the asthenospheric layer (e.g., associated with thermal or chemical heterogeneities or pockets of melt) or associated with lateral variations in lithospheric thickness (e.g., near a ridge or a cratonic "edge"). In some engineering applications, for example, the presence of a shear flow beneath an open fluid-filled "cavity" can produce circulatory flow within the cavity at low Reynolds numbers (e.g., Shen and Floryan, 1985; Pakdel et al., 1997; Shankar and Deshpande, 2000). Applied to the asthenosphere, this "shear-driven cavity flow" may produce a type of upwelling that is not associated with any convective process. Instead, the driver for this type of upwelling is the relative motion between the plates and mantle; upwelling flow is excited in this case by viscosity heterogeneity, rather than density heterogeneity (e.g., Fig. 1). In this study,

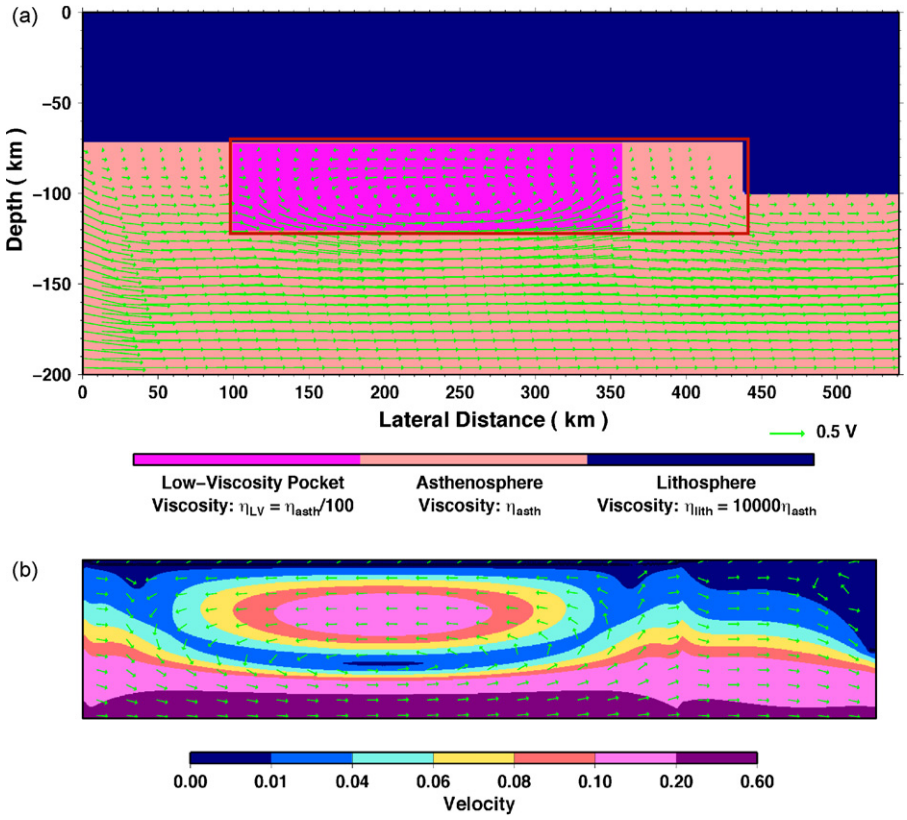

Fig. 1. Viscous flow calculation showing the effect of both a low viscosity "pocket" and a lithospheric step on asthenospheric shear flow. In (a), arrows indicate velocity direction and magnitude (note scale arrow showing 0.5 *V*, where *V* is the magnitude of the velocity imposed on the asthenospheric base at 200 km), while colors indicate viscosity variations. A detailed view of the red-outlined box in (a) is shown in (b), where arrows indicate velocity direction and colors indicate magnitude of velocity. In (a) and (b), amplitudes of velocity are given as a fraction of the velocity that drives the shear flow at the base of the asthenosphere.

we examine how asthenospheric shear flow may combine with asthenospheric or lithospheric viscosity heterogeneity to produce upwelling flow in the asthenosphere. We then examine the dynamical situations where this type of "shear-driven upwelling" (SDU hereafter) may generate mantle upwelling, and thus intraplate volcanism.

2. Lithospheric viscosity variations: shear-driven cavity flow

We first examine the response of asthenospheric shear flow to a variation in the basal topography of the lithosphere. Such variations are expected in the vicinity of mid-ocean ridges, continental rifts, and cratonic roots. To describe asthenospheric shear flow beneath these features, we turn first to the engineering literature, where the fluid mechanics of highly viscous (low Reynolds number) flows have been well studied. Here we examine flow beneath lithospheric thickness variations in terms of the classic engineering problem known as "lid-driven" (e.g., Pakdel et al., 1997; Shankar and Deshpande, 2000; Gürcan, 2005) or "shear-driven" (e.g., Shen and Floryan, 1985; Pakdel et al., 1997; Shankar and Deshpande, 2000) flow within a cavity. For the shear-driven cavity flow, most published literature deals with a rectangular cavity added to one wall of a channel (Fig. 2); motion of the opposite wall generates shear within the channel that excites flow within the cavity.

2.1. Model setup

We study cavity flow using the finite element code *ConMan* (King et al., 1990), which is designed for two-dimensional study of incompressible viscous flow within the Earth's mantle. We generate asthenospheric shear flow (e.g., Fig. 1) by imposing rigid velocity boundary conditions at the surface and a dimensionless velocity V on the base of an asthenospheric channel that is $H_{asth} = 100$ km thick and contains fluid of viscosity η_{asth}. Above the asthenosphere lies a lithospheric layer with a high viscosity of $10{,}000\eta_{asth}$, which serves to impose stationary conditions on the top of the asthenospheric channel (meaning that we are studying shear flow in the reference frame of the surface plate; V then represents the full velocity contrast across the asthenosphere). We embed a cavity (with width W_C, height H_C, and viscosity η_C) within the lithospheric layer (Fig. 2) in order to study flow patterns induced in the cavity by the driven asthenospheric shear. The cavity height and width is made dimensionless using the aspect ratio A_C and the asthenospheric thickness ratio T_C,

$$A_C = \frac{W_C}{H_C} \quad \text{and} \quad T_C = \frac{H_{asth}}{H_{asth} + H_C} \tag{1}$$

T_C expresses the relative asthenospheric thicknesses with and without the cavity. To implement the viscosity heterogeneity associated with the cavity, we combine an imposed temperature field with temperature-dependent viscosity. Because the former is nearly discontinuous, viscosity varies rapidly between the cavity and the lithosphere and/or asthenosphere (for cases where $\eta_C < \eta_{asth}$). Such rapid variations in viscosity between regions have been investigated previously using *ConMan* (e.g., King and Hager, 1990), and allow both velocity and stress to vary continuously across the boundary, while velocity derivatives (i.e., strain-rates) are not continuous. A 30 km buffer zone (Fig. 2) is included between the cavity walls and the side boundaries; tests showed that this separation was sufficient to remove any sidewall influence on flow within the cavity. Side boundary conditions are stress-free in the horizontal direction and no-slip in the vertical direction, which permit free horizontal flow into and out of the calculation. The calculations performed here use resolutions of 0.5, 1.0, or 2.0 km (depending on the cavity size), and thus require up to 300,000 finite elements.

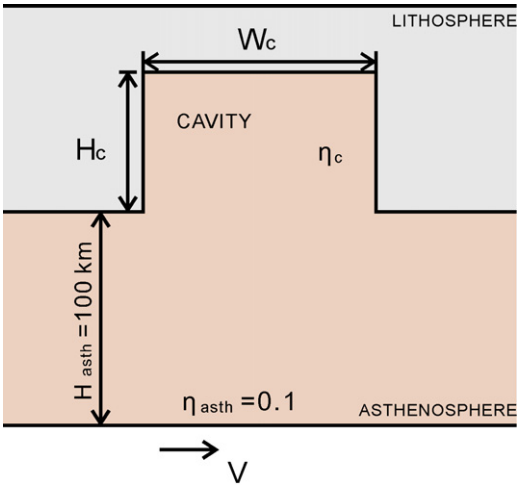

Fig. 2. Cartoon drawing of asthenospheric shear flow (driven by an imposed basal velocity of V) beneath a stationary lithosphere that features a "cavity" of variable height H_C and width W_C and viscosity η_C.

2.2. Numerical results

If the cavity viscosity is equal to that of the surrounding asthenospehre ($\eta_C = \eta_{asth}$), the flow patterns within the cavity are largely determined by the cavity dimensions. For narrow cavities, we observe a circulatory flow pattern that fills the entire cavity ($A_C = 2$ and $T_C = 0.85$, Fig. 3a). This circulation is driven from below by asthenospheric shear and includes shear-driven upwelling (SDU) flow along the downstream wall of the cavity, return flow along the cavity ceiling, and downwelling along the upstream wall. As the aspect ratio grows ($A_C = 4$ and $T_C = 0.85$, Fig. 3b), the walls of the cavity become increasingly separated and the returning flow along the cavity ceiling diminishes. In this case, circulatory flow and associated SDU is confined to the two inner corners of the cavity while the rest of the cavity becomes filled with a broad widening of the background asthenospheric shear flow. As the cavity widens further ($A_C = 6$ and $T_C = 0.85$, Fig. 3c), the penetration of the asthenospheric shear flow into the cavity dominates the cavity flow field. Note that in this case, SDU occurs on the downstream side of the cavity as part of the corner circulation, and on the upstream side of the cavity as part of the widening shear flow. These patterns of cavity flow have been documented previously (Shankar and Deshpande, 2000) in laboratory (Shen and Floryan, 1985) and analytical (Gürcan, 2005) studies.

We characterize the full range of cavity flow behavior by varying A_C and T_C. By examining the maximum upwelling velocity within the cavity (Fig. 4a), we find that the fastest upwelling flow occurs for the widest (large A_C) and deepest (small T_C) cavities. As discussed above, a wide cavity permits penetration of the asthenospheric shear flow into the cavity; a deeper cavity requires a more extensive penetration of this flow, and thus permits a faster upwelling velocity. By examining the horizontal velocity at the cavity centerline at a point 10% of the cavity thickness from the cavity ceiling (Fig. 4b), we can determine the pattern of flow in the cavity. For narrow cavities (small A_C), these velocities are negative and represent return flow from the cavity circulation (Fig. 3a). For wider cavities, these velocities are positive and represent penetration of asthenospheric shear flow into the cavity (Fig. 3c). The boundary between these two regimes occurs when the horizontal velocity is approximately zero at this depth (Fig. 4b). Shen and Floryan (1985) showed that this transition occurred at an aspect ratio of about 3; we find that

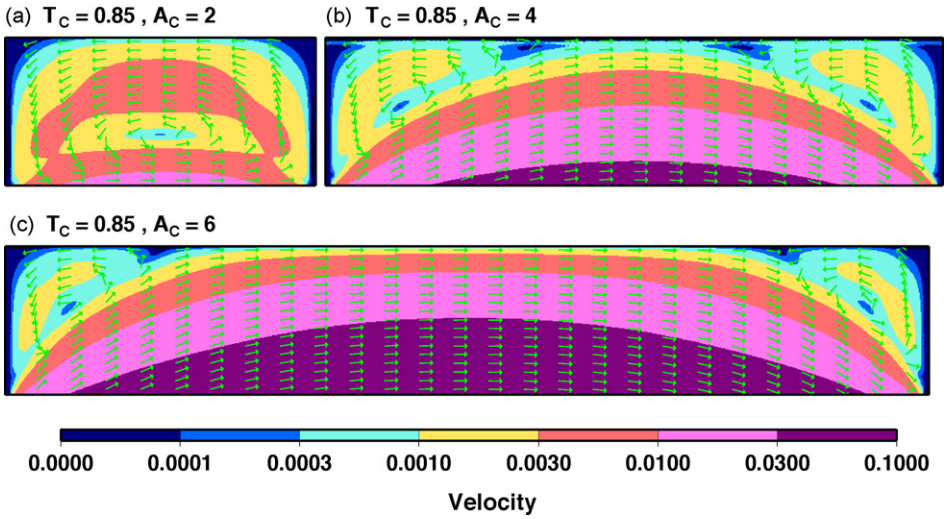

Fig. 3. Calculations of the flow field within the cavity depicted in Fig. 2, for three different aspect ratios of the cavity and $T_C = 0.85$. Arrows indicate direction of flow, colors indicate velocity magnitude as fraction of V, the imposed velocity at the base of the asthenosphere. Three different patterns of flow are shown. (a) For aspect ratio $A_C = 2$, the cavity is narrow enough that the asthenospheric shear flow cannot penetrate into the cavity. Instead, a closed circulation develops within the cavity, with upwelling occurring along the downstream wall of the cavity. (b) As the cavity widens, the asthenospheric shear flow begins to penetrate into the cavity. At about $A_C = 4$ (shown here), this flow reaches the cavity lid, eliminating the closed circulation that occurs for smaller aspect ratios. Instead, individual circulatory cells develop in the corners of the cavity. (c) For larger aspect ratios ($A_C = 6$ is shown here) the asthenospheric shear flow dominates in the center of the cavity, but circulation persists in the cavity corners.

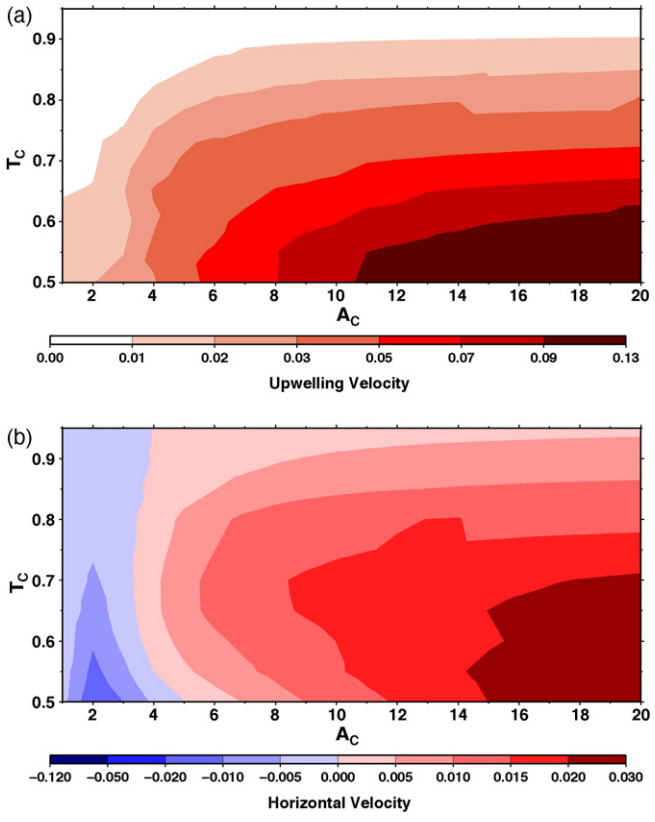

Fig. 4. Measurements of (a) the maximum upwelling flow within the cavity and (b) the horizontal velocity at a point 10% of H_C from the top of the cavity midpoint, as a function of the aspect ratio A_C and the cavity thickness ratio T_C. The style of flow can be determined from the direction of horizontal flow in (b), where blue negative values indicate the presence of a closed circulation in the cavity (as in Fig. 3a), and red positive values indicate a cavity flow field dominated by shear flow (as in Fig. 3c). The boundary between these flows (lightest blue and pink interface) indicates the transition between these two flows (as in Fig. 3b).

the critical aspect ratio depends on T_C, but is between 3 and 4 for $T_C > 0.55$. Shen and Floryan's (1985) study assigns cavity dimensions consistent with $T_C \sim 0.94$, but employ a Poiseuille-Couette flow field that amplifies shear near the cavity mouth, leading to a somewhat smaller effective T_C. For $T_C \sim 0.7$, we find a critical aspect ratio close to (but slightly larger than) the value of ~3 that Shen and Floryan (1985) observed, indicating a broad consistency of our results with the engineering literature.

Because asthenosphere within a lithospheric cavity is likely to reside closer to the solidus than deeper asthenosphere, its viscosity may be lower (Schmeling and Bussod, 1996), particularly if it is anomalously hot (e.g., Korenaga and Jordan, 2002) or wet (e.g., Hirth and Kohlstedt, 1996). To test how low cavity viscosities affect SDU, we also examined the case where η_C is smaller than η_{asth} by a factor of 10 (Fig. 5). The lower viscosity in the cavity causes more of the deformation of the system to move from the channel into the lower-viscosity cavity. This enhanced deformation of the cavity fluid allows circulatory flow within the cavity for higher aspect ratios (compare Fig. 5b and Fig. 4b), and generally increases the magnitude of SDU for the circulatory flow regime (compare Fig. 5a and Fig. 4a).

2.3. Shear-driven cavity flow within Earth's asthenosphere

On Earth, cavities within the lithosphere are found beneath mid-ocean ridges and continental rifts. However, because plate spreading is associated with both of these tectonic environments, the presence of persistent asthenospheric shear in one direction is unlikely. Furthermore, volcanism in these systems can already be well explained by passive upwelling associated with localized extension. Nevertheless, if spreading ceases or becomes overwhelmed by a shear flow induced by global mantle flow, then the sub-lithospheric cavities associated with mid-ocean ridges or continental rifts might serve as hosts to SDU. The "edge" of a thick craton, if present above asthenospheric shear, may also excite SDU, and can be examined in terms of shear-driven cavity flow if we assume a very wide cavity.

To evaluate the capacity of these geometrical configurations to produce SDU, we estimate the ratios T_C and A_C, and refer to Figs. 4a and 5a to estimate the maximum rate of SDU relative to the

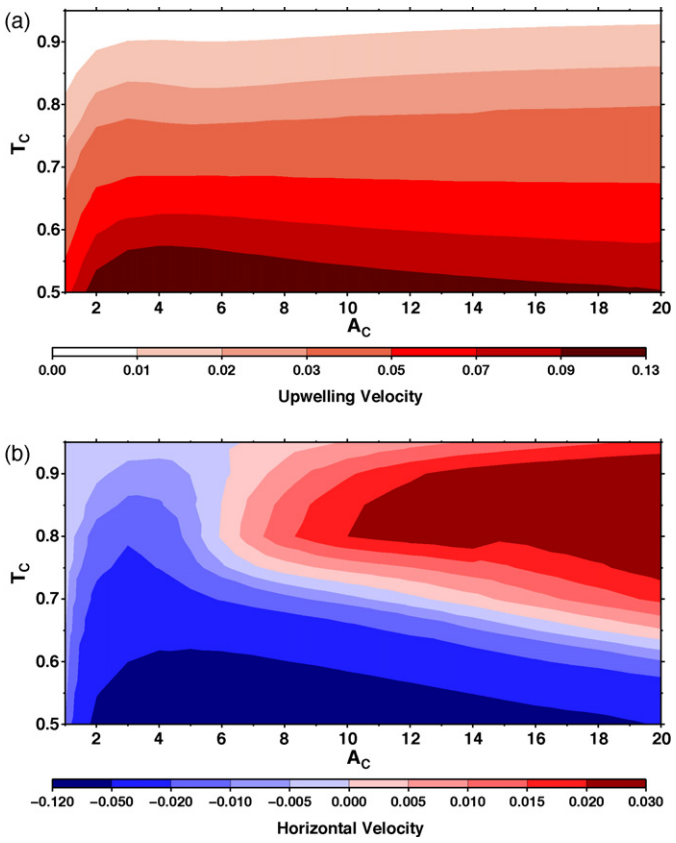

Fig. 5. Similar to Fig. 4, but for a low viscosity fluid within the cavity. Here, the cavity fluid is 10 times less viscous than the fluid of the rest of the asthenosphere.

driving shear flow. To evaluate the style of cavity flow, we refer to Figs. 4b and 5b. Full circulation within the cavity is indicated by the blue regions of these figures; in these cases SDU should occur on the "downstream" wall of the cavity (e.g., Fig. 3a; here and below, "downstream" refers to the direction of the shear flow with respect to the stationary plate; "upstream" is the opposite direction). In the red regions of these figures, flow primarily follows the contours of the lithospheric base (e.g., Fig. 3c). Although upwelling does occur as the shear flow enters the cavity, the associated upwelling is generally diffuse and therefore slow. These cases also show that small circulatory "vortices" also occur within the inside corners of the upstream-facing steps (e.g., Fig. 3c). These vortices produce SDU with amplitudes only ~0.1% of the shear velocity amplitude, and will only occur if these interior corners are sufficiently sharp. Therefore, we do not expect significant SDU to be associated with these interior vortices for most geologic scenarios, which likely feature more gradually sloping edges and rounded corners. As a result, we will only consider SDU from a cavity flow to be significant if there is a closed circulation within the cavity (as in Fig. 3a), as indicated by the blue regions of Fig. 4b and c.

For a mid-ocean ridge, we estimate T_C and A_C by noting that the thickness of the oceanic lithosphere increases rapidly away from the ridge. At 10 Myr, the base of the lithosphere (approximated by the 1000 °C isotherm) should be ~30 km deep (e.g., Stein and Stein, 1992). For the slowest spreading ridges (e.g., the mid-Atlantic ridge, which spreads at ~2 cm/yr in places), the two 10 Myr isochrons are about 400 km apart. This yields $T_C \sim 0.9$ if the base of the asthenosphere is 300 km deep, and $A_C \sim 13$. The upwelling rate associated with SDU in this cavity is rather slow (Fig. 4A) and does not involve circulatory flow (it is in the red area of Fig. 4b), primarily because the cavity depth is small relative to the asthenospheric thickness, and does not induce significant velocity gradients near the cavity base. Slow and non-circulating flows are expected even if the cavity is filled with low-viscosity fluid (Fig. 5), as expected if excess heat or melting is present beneath the ridge. Therefore, shear-driven cavity flow may only form beneath a ridge if asthenospheric shear becomes concentrated within a much narrower (~100 km, yielding $A_C \sim 3$) region immediately beneath the ridge, perhaps via viscous layering of the asthenosphere. Even so, the edges of such a cavity are likely to be sloping, which would tend to make the cavity effectively shallower and wider, both of which tend to diminish circulatory flow.

Continental rifting may provide a greater opportunity for SDU because existing continental lithosphere can be thicker than new oceanic lithosphere, and therefore produce a deeper cavity. For example, tomographic studies of the Rio Grande rift (West et al., 2004), show a ~200 km wide low-velocity anomaly extending 100–200 km beneath the surface and surrounded by a 100 km thick layer with a faster velocity anomaly (van Wijk et al., 2008). Again assuming a 300 km depth to the asthenospheric base, we estimate $T_C \sim 0.67$ and a cavity aspect ratio of only about 2. This combination of parameters allows for circulatory flow within the cavity (blue regions of Fig. 4b and 5b), with amplitudes of up to about 4% of the shear flow amplitude if the cavity is filled with low-viscosity fluid (Fig. 5a). Since the amplitude of asthenospheric shear cannot be greater than the rate of plate motions, which can be up to about 5 cm/yr for continental plates, then SDU within a continental rift could induce upwelling rates of up to about 0.2 cm/yr within the rift, particularly against the downstream wall of the sublithospheric rift cavity. Again, the amplitude and likelihood of such upwelling may be diminished if the slopes of the cavity walls are significant relative to the size of the cavity, as they may be for most rift systems.

We also investigate the possibility of SDU forming against the edge of a large variation in lithospheric thickness, such as the side of a cratonic root, by considering only one wall of a large aspect ratio cavity (e.g., $A_C > 10$, Figs. 4 and 5). Cratons may penetrate as deeply as 200–300 km or more (e.g., Jaupart and Mareschal, 1999), which indicates $T_C < 0.5$ if the surrounding lithosphere is 100 km thick and the asthenospheric base is 300 km deep. For a uniform viscosity asthenosphere, the flow field within the "cavity" (in this case the portion of the asthenosphere bounded by the step) is non-circulatory (red area of Fig. 4b) and simply responds to the changing asthenospheric thickness; the shear flow is downward beneath an upstream-facing step and upward beneath a downstream-facing step (Fig. 3c). If the asthenosphere is layered, however, such that the fluid next to the step is low-viscosity, then our calculations show that a large step induces a "return flow" in the upper asthenosphere (Fig. 5b is blue for $T_C < 0.6$). In this case, we expect upwelling against an upstream-facing step (e.g., Fig. 3a, but for large aspect ratio) with an amplitude that can be 10% of the shear amplitude (Fig. 5a), or 0.5 cm/yr for a 5 cm/yr shear flow. Any slope to a cratonic "edge" likely occurs on wavelengths shorter than those of the craton itself, and therefore should not affect the presence of upwelling flow in the vicinity of a cratonic edge. However, such sloping basal topography should cause any induced upwelling to become more laterally distributed than it is for the vertical cavity walls modeled here, which would reduce the maximum rate of upwelling.

Finally, rapid variations in lithospheric thickness may occur in non-cratonic regions as well, such as near the Basin and Range province, where a sharp ~50 km increase in lithospheric thickness has been documented (Zandt et al., 1995) near volcanism that seems to arise from asthenospheric melting (Wang et al., 2002). When added above asthenosphere that is at least 150 km thick, we estimate $T_C > 0.7$ for these non-cratonic lithospheric steps. These shallower steps do not produce a return flow in the asthenosphere (Fig. 4b), even for a low-viscosity upper asthenosphere (Fig. 5b). Thus, although large steps ($T_C > 0.5$) may produce SDU for

either upstream- or downstream-facing orientations, smaller steps ($T_C > 0.7$) will only generate SDU if they face downstream.

3. Asthenospheric viscosity variations: circulatory flow in a low-viscosity "pocket"

A geophysically interesting variation of the shear-driven cavity flow, which has not been explored in the engineering literature, involves relaxing the rigidity of the cavity-containing layer. In this case, the "cavity" becomes a region of relatively low-viscosity that is embedded within the shearing layer (Fig. 6). The viscosity heterogeneity in this case may result from the presence of "pockets" of mantle with unusually high temperature, volatile concentration, or melt fraction, or small grain size, which produce regions of anomalously low viscosity within a shearing asthenospheric layer. Here we examine patterns of viscous flow within a low-viscosity "pocket" that is subjected to rapid asthenospheric shear.

3.1. Model setup

To study the response of asthenospheric viscosity heterogeneity to imposed shear flow, we again set up viscous flow calculations using the finite element code *ConMan* (King et al., 1990). As before, we induce shear flow in a 100 km thick asthenospheric layer (viscosity η_{asth}) by imposing a basal velocity V while holding the high-viscosity lithosphere (viscosity $10{,}000\eta_{asth}$) stationary (Fig. 6). To introduce lateral heterogeneity into the asthenospheric layer, we assign low viscosities ($\eta_{LV} < \eta_{asth}$, implemented similarly to the lithospheric cavity) to a rectangular region (width W_{LV} and height H_{LV}) that is located a depth D_{LV} beneath the base of the lithosphere (Fig. 6). We thus define the dimensionless aspect ratio A_{LV}, height H'_{LV}, depth D'_{LV}, and viscosity η'_{LV} of the low-viscosity region using,

$$A_{LV} = \frac{W_{LV}}{H_{LV}}, \quad H'_{LV} = \frac{H_{LV}}{H_{asth}}, \quad D'_{LV} = \frac{D_{LV}}{H_{asth}}, \quad \text{and} \quad \eta'_{LV} = \frac{\eta_{LV}}{\eta_{asth}}. \tag{2}$$

We use 1 km resolution for these calculations, and extend the studied box by 100 and 20 km on the upstream and downstream sides of the pocket, respectively. To maintain a basic shear flow pattern within the asthenosphere for all cases, we utilize free flow conditions on the left side, and impose a simple Couette flow (for a uniform viscosity layer) condition on the right side (Fig. 6). This condition prevents deviations from a governing background shear flow that occasionally occur when the low-viscosity pocket occupies a large fraction of the asthenospheric volume.

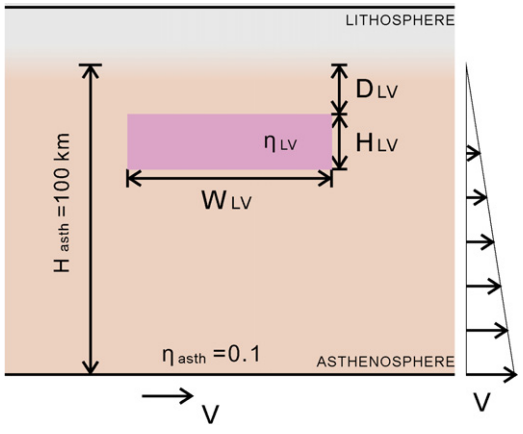

Fig. 6. Cartoon drawing of asthenospheric shear flow (driven by an imposed basal velocity of V) with an embedded "pocket" of low-viscosity fluid (the Low Viscosity Region, LVR) of variable height H_{LV}, width W_{LV}, depth D_{LV}, and viscosity η_{LV}, as shown.

3.2. Numerical results

To examine the variety of flow patterns that are excited within the low viscosity pocket by the shear flow, we first varied both the height H'_{LV} and aspect ratio A_{LV} of the pocket region, while keeping the surface of the pocket flush with the base of the lithosphere ($D'_{LV} = 0$). For some cases, we find that circulatory flow develops within the pocket (Fig. 7b) because the shear flow imposes a horizontal velocity condition on the base of the pocket while the surface of the pocket is held fixed by the presence of the high-viscosity stationary lithosphere. Because the fluid in the pocket is low-viscosity, these two external forces produce a circulatory flow within the pocket, similar to what occurs for the cavity flow described above. Superimposed on this circulatory flow, however, is the background shear flow of the surrounding asthenospheric layer. If the low-viscosity pocket's vertical extent spans a large fraction of the asthenosphere height (i.e., $H'_{LV} > 0.7$), then this background shear flow tends to overwhelm the circulatory flow. Alternatively, a wider and thinner pocket causes the system to behave as a layered structure, concentrating asthenospheric shear within the pocket where the low-viscosity permits more rapid deformation.

As an example, first consider flow in a cavity extending through 80% of the asthenosphere ($H'_{LV} = 0.8$ and $A_{LV} = 4$, Fig. 7a). In this case the background shear flow dominates and there is no return flow within the cavity, but the presence of weak circulatory behavior is evident by upward- and downward-deflected velocities on the upstream and downstream sides of the pocket (respectively). On the other hand, if the pocket aspect ratio is less than about 2 ($A_{LV} < 2$), then the pocket becomes too small for a significant circulation to develop in response to the background shear. This is because circulatory flow requires the pocket fluid to turn around the corners of the pocket, and for smaller pockets the energy required for this turning deformation become prohibitive. Thus, smaller pockets exhibit shear deformation similar to the rest of the asthenosphere (Fig. 7c), rather than generating their own internal circulation. These examples show that we should expect circulatory flow (e.g., as in Fig. 7b) to be excited within the pocket only for a limited range of pocket geometries. Because pocket deformation depends strongly on the viscosity of the pocket, we expect this range to depend on the rheological contrast between the pocket and the background asthenosphere ($\eta'_{LV} = \eta_{LV}/\eta_{asth}$).

To look for the geometrical conditions that lead to circulatory pocket flow, we measured the maximum upwelling velocity within the pocket region (Fig. 8a–d) and the horizontal velocity at a location 10% of H'_{LV} below the top of the pocket (Fig. 8e–h). For a large viscosity contrast between the pocket and the asthenosphere ($\eta'_{LV} = 0.01$, as in Fig. 7), we detect upwelling flow for $A_{LV} > 3$ and $0.1 < H'_{LV} < 0.7$ (Fig. 8a). The presence of a negative horizontal velocity near the top of the pocket confirms that this upwelling is part of a circulatory flow within the pocket (Fig. 8e). For a pocket that is 100 times less viscous than the asthenosphere ($\eta'_{LV} = 0.01$), the maximum upwelling velocity in the pocket can be up to about 20% of the maximum shear velocity contrast for $A_{LV} > 6$ and $0.3 < H'_{LV} < 0.5$ (Fig. 8a). As the viscosity of the pocket increases toward the asthenosphere viscosity, the pocket geometries that produce circulatory flow remain approximately the same, but the vigor of circulatory flow within the pocket decreases (Fig. 8). For $\eta'_{LV} = 0.03$, the maximum upwelling velocity is less than 10% of the shear velocity contrast (Fig. 8b), while at $\eta'_{LV} = 0.1$ it has decreased to less than 3% (Fig. 8c) and is undetectable for $\eta'_{LV} = 0.3$ (Fig. 8d). The amplitudes of the horizontal velocities near the top of the pocket confirm these trends (Fig. 8e–h), as does a plot of the

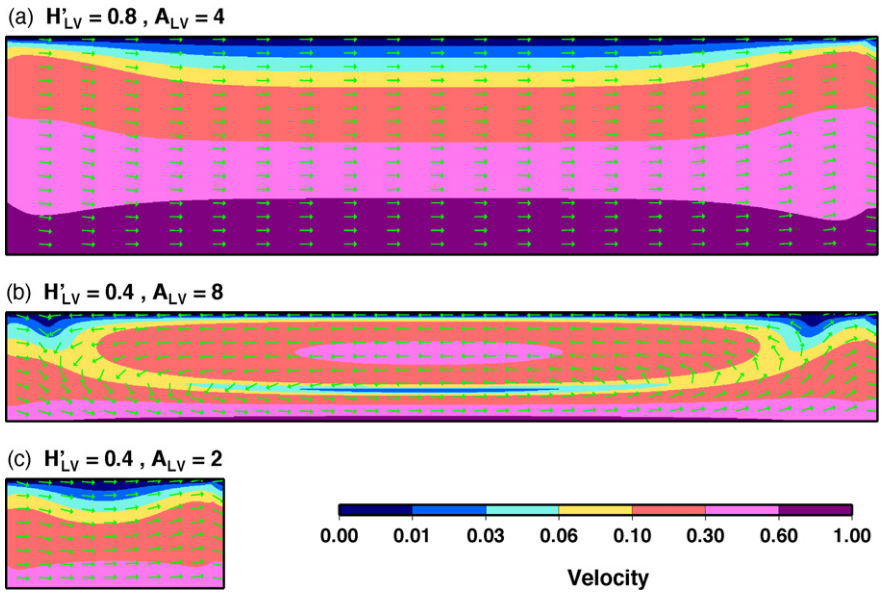

Fig. 7. The flow field within a pocket of low-viscosity fluid (as depicted in Fig. 6) with viscosity $\eta'_{LV} = \eta_{LV}/\eta_{\text{asth}} = 0.01$, for three different choices of pocket aspect ratio A_{LV} and dimensionless height H'_{LV}. Arrows show the flow field direction, while colors present the magnitude of flow.

maximum upwelling velocity observed (for any H'_{LV} or A_{LV}) as a function of η'_{LV} (Fig. 9, red line).

Finally, we find that the positioning of the pocket deeper within the asthenospheric layer (increasing D'_{LV}), tends to decrease the magnitude of circulatory flow within the pocket (Fig. 9). This is because the lithosphere forms a solid unmoving upper boundary for the pocket if $D'_{LV} = 0$, but the deformability of the fluid above the pocket increases as D'_{LV} increases. If the fluid above the pocket is deformable, then the shear flow can redistribute itself into the fluid above the pocket. In this case, the pocket rides along with the flow, and the circulatory deformation within the pocket is diminished.

3.3. Interaction of a low-viscosity "pocket" with a lithospheric step

Because SDU is produced by shear flow acting on both lithospheric steps and asthenospheric pockets, we can ask whether these types of flow could act together to augment upwelling rates. To test this, we placed a low-viscosity pocket (Fig. 1, using $A_{LV} = 5$, $H'_{LV} = 0.3$ or 0.4, and $\eta'_{LV} = 0.01$) upstream of a lithospheric step function (height 30 km) and measured the maximum upwelling as before. We found that as the pocket gets closer to the step, the maximum upwelling velocity decreases slightly. This is because near the lithospheric step, the pocket upwelling occurs where the step forces the flow downward (Fig. 1); the two flows partially cancel. Similarly, if the pocket is located downstream from a downstream-facing lithospheric edge (e.g., if the direction of shear is reversed in Fig. 1), then by symmetry the upwelling flow around the step would partially cancel the downwelling flow of (now reversed) circulation within the low-viscosity pocket. We found that the effect of combining the two flows was larger for thinner asthenosphere because the relative deflection of the flow by the step is larger. However, the fastest upwelling is generated by the low-viscosity pocket, and as a result pocket flow is only slightly affected (by at most about 20%, and only if the pocket is within 40 km of the lithospheric step for the example in Fig. 1) by the presence of a lithospheric step.

3.4. Low-viscosity pocket flow within Earth's asthenosphere

Tomographic studies of the asthenosphere show low-velocity anomalies with a variety of geometries and sizes. For example, detailed tomography of the mantle beneath the Basin and Range region shows several regions with anomalously slow seismic velocity that were first observed by Humphreys and Dueker (1994), but appear differently in various tomographic studies since. Dueker et al. (2001) show low-velocity regions that range in width from about 100 to 300 km, and in height from about 50 to 200 km; similarly narrow pockets of slow seismic velocity have since been detected by Moschetti et al. (2007). Considering an asthenospheric layer that is ~200 km thick, these values indicate that H'_{LV} may vary between 0.25 and 1.0, and A_{LV} between 0.5 and 6. Other, lower resolution, tomographic images show wider anomalies, even in the basin and range region (e.g., van der Lee and Frederiksen, 2005), which indicates that a wide variety of pocket aspect ratios are possible. The depth of the possible anomalies beneath the lithosphere is not well constrained, but Dueker et al. (2001) show low velocity anomalies that extend up to ~50 km depth, close to others' estimates of the depth to the lithospheric base (e.g., Zandt et al., 1995). Thus, D'_{LV} may be as small as zero for the low-velocity anomalies detected by Dueker et al. (2001). Taken together, these constraints allow for the possibility that the interaction of asthenospheric shear flow with low-velocity anomalies may produce localized upwelling flow on the downstream side of these anomalies with amplitudes up to 20% of the shear flow magnitude (Fig. 8a). If we consider 5 cm/yr of shear flow, then the rate of upwelling flow could be up to 1 cm/yr. This estimate can be regarded as an upper bound on the rate of asthenospheric upwelling because the low-viscosity region must be more than 100 times less viscous than the surrounding asthenosphere ($\eta'_{LV} = 0.01$) and approximately 80 km high by 480 km wide (yielding $A_{LV} = 6$ and $H'_{LV} = 0.4$ for a 200 km thick asthenosphere). These sizes are close to the extreme values estimated from Dueker et al.'s (2001) images and most anomalies feature a smaller aspect ratio.

The magnitude of the viscosity heterogeneity that could be associated with low-viscosity pockets is not clear. The magnitude of the slow velocity anomalies in Dueker et al.'s (2001) images are up to about −1.5%. For a background shear wave speed of 4.5 km/s, this indicates a shear velocity anomaly of about 70 m/s, which is half that of the slow-velocity anomalies of ~150 m/s estimated for the same region by van der Lee and Frederiksen (2005). If the anomaly has a thermal origin, then we can convert this 70–150 m/s velocity anomaly to a 10–20 kg/m^3 density anomaly and then to a 100–200 K thermal anomaly (assuming a density conversion factor

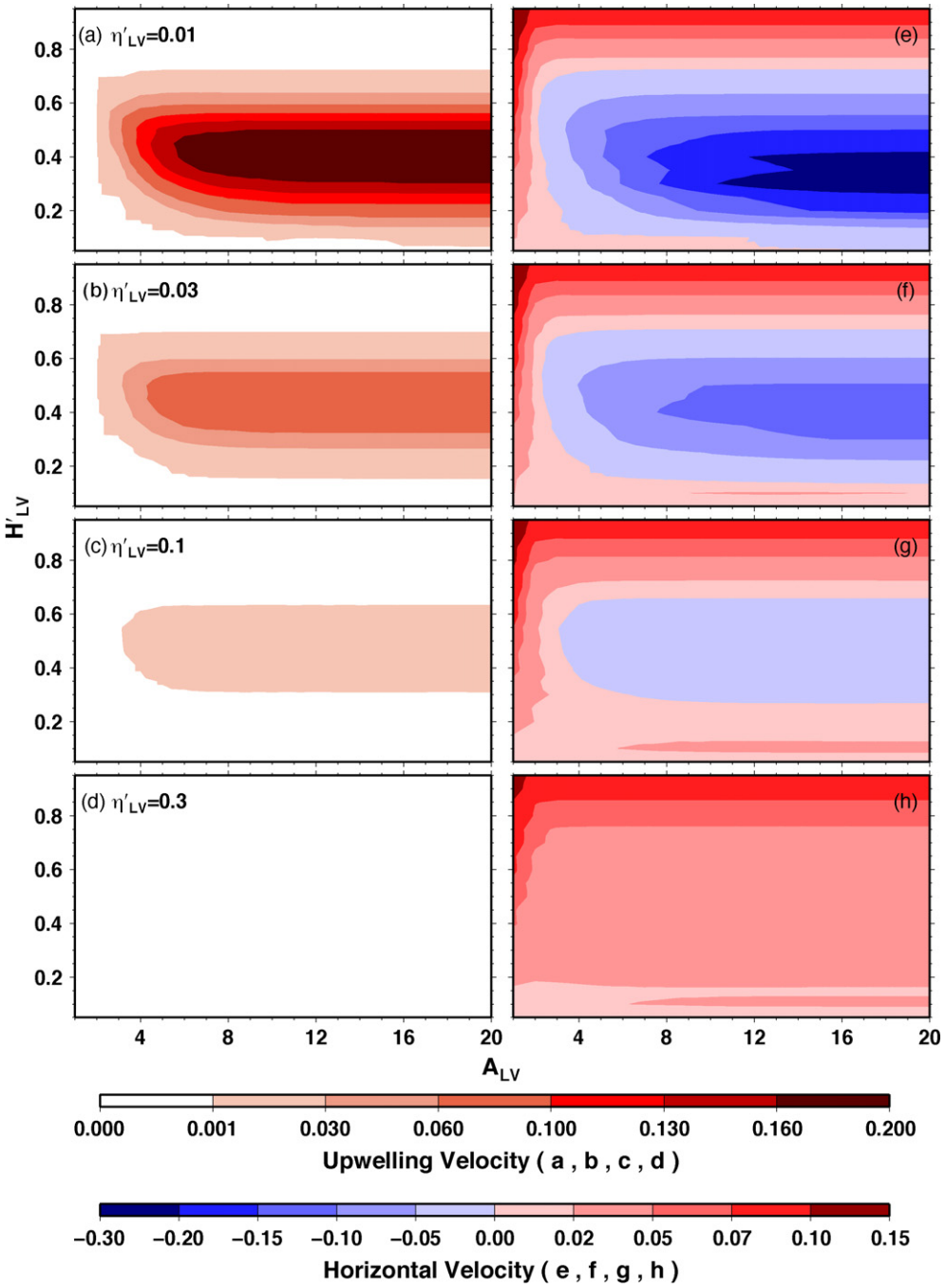

Fig. 8. Summary (similar to Fig. 4) of the upwelling flow and return flow within the low viscosity pocket. Here the pocket viscosity is $\eta'_{LV} = \eta_{LV}/\eta_{asth} = 0.01$ for (a and e), 0.03 for (b and f), 0.1 for (c and g), and 0.3 for (d and h). As in Fig. 4a, parts (a–d) show the maximum upwelling velocity in the pocket. As in Fig. 4b, parts (e–h) show the horizontal velocity at a depth 10% of H_{LV} from the top of the pocket, where red (positive) indicates downstream flow (as in Fig. 7a and c) and blue (negative) indicates circulatory flow within the pocket (as in Fig. 7b).

of 0.15 g cm^3 km^{-1} s (e.g., Conrad et al., 2007), a thermal expansivity of 3×10^{-5} K^{-1}, and a background density of 3300 kg/m^3). Because temperature-dependent viscosity tends to produce an order of magnitude decrease in viscosity for every 100 °C of temperature increase (e.g., Kohlstedt et al., 1995), a thermal anomaly of up to 200 °C could be up to 2 orders of magnitude less viscous than its surroundings, giving $\eta'_{LV} = 0.01$. As discussed above, pockets with this viscosity contrast could produce SDU with upwelling rates as large as 1 cm/yr if driven by 5 cm/yr of asthenospheric shear.

If, on the other hand, the anomalies are associated with melting, then a melt fraction of 0.5–1% would be associated with a 1.5–3.0% shear-wave velocity anomaly (assuming a conversion factor of 3.3% S-wave anomaly per percent melt fraction (Schmeling, 1985), as others have used (e.g., Toomey et al., 1998; Rychert et al., 2005)). Generally, an order of magnitude decrease in viscosity, which is necessary to produce SDU (Fig. 8), requires at least a ∼4% melt fraction (e.g., Hirth and Kohlstedt, 1995a,b), although melt fractions of only a few percent may be required for small grain sizes (Kohlstedt and Zimmerman, 1996). On the other hand, some studies have suggested that the presence of melt may tend to dehydrate the solid minerals, which could increase net viscosity, not decrease it (Karato, 1986). Thus, partial melt, especially occurring

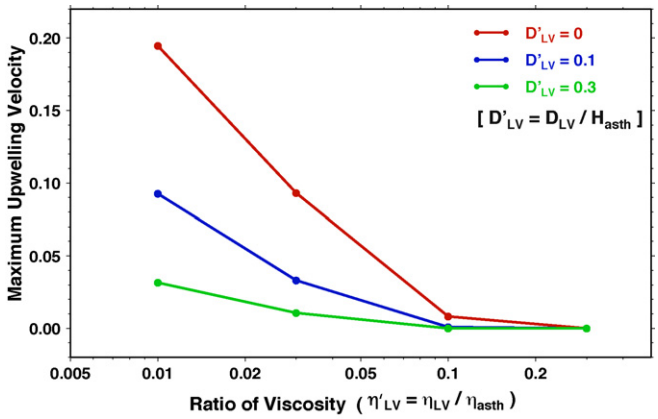

Fig. 9. The maximum upwelling velocity as a function of the pocket viscosity $\eta'_{LV} = \eta_{LV}/\eta_{\text{asth}}$ and the depth D'_{LV} of the top of the pocket beneath the lithospheric base ($D'_{LV} = 0$ for red, 0.1 for blue, and 0.3 for green).

within hydrated asthenosphere, is not likely to produce a sufficient reduction in viscosity to generate SDU, unless this melt is accompanied by a thermal anomaly or grain-size reduction that also reduces viscosity.

Finally, a heterogeneous concentration of water or other volatiles may produce low-viscosity pockets with anomalously slow seismic velocity. Hydration near the lithospheric base can produce a velocity drop of up to about 4.3% (e.g., Rychert et al., 2005, based on Karato and Jung, 1998 and Gaherty et al., 1999). Because the effect of hydration (at a level of 810 ± 490 H/10^6 Si) on upper mantle viscosity can be more than a factor of 100 (Hirth and Kohlstedt, 1996), hydration of olivine should decrease viscosity sufficiently to produce SDU. Thus, it is possible that low-viscosity "pockets" of hydrated asthenosphere may lead to SDU if subjected to vigorous asthenospheric shear. Other compositional heterogeneity, possibly associated with other volatiles, grain-size reduction, or a variable melt extraction history, may also contribute to the total viscosity heterogeneity. Thus, there are several mechanisms (thermal, melting, volatile, chemical, or grain-size) that could contribute to a factor of ~100 decrease in viscosity within "pockets" of asthenospheric mantle. We estimate that SDU produced by the action of asthenospheric shear on these regions can produce upwelling rates of up to 1 cm/yr. If asthenospheric source rocks are close to solidus, this upwelling can generate melting, inducing melting instabilities and/or intraplate volcanism.

4. Upwelling, melting, and surface volcanism

Viscosity heterogeneity in the asthenosphere or lithosphere, which is necessary to produce SDU, is generally caused by thermal, melting, or volatile anomalies that are also associated with anomalously low mantle density. Thus SDU may be at least partially influenced by upwelling driven by density heterogeneity linked to the viscosity heterogeneity. If externally imposed shear is sufficiently large, then SDU will overwhelm any buoyancy-driven flows. On the other hand, buoyancy-driven flow will dominate if the shear flow is sufficiently weak. In between, upwelling flow will be driven by a combination of both shear-driven and density-driven mechanisms, which may interact and potentially augment each other. Below we determine the scenarios under which SDU controls, rather than merely augments, asthenospheric upwelling and volcanism. For the cases where SDU is dominating, we estimate the rates of asthenospheric melting and surface volcanism that would be expected.

4.1. Upwelling beneath lithospheric cavities and steps

We have already shown that SDU in an optimally shaped lithospheric cavity or step may be at most about 4% or 10% of the imposed shear magnitude, respectively. For these cases, the viscosity heterogeneity that drives the SDU is associated with the lithosphere–asthenosphere boundary. If this boundary results from temperature heterogeneity, the high-viscosity lithosphere will be denser than the underlying asthenosphere, and therefore prone to convective instability. The thickness of the basal lithosphere that actually participates in sub-lithospheric small-scale convection depends strongly on the variation of viscosity within the dense lithosphere (Conrad and Molnar, 1999). If viscosity varies only weakly with temperature, then a significant portion of the lower lithosphere may be weak enough to be removed by dripping instabilities and subsequently replaced by rising asthenosphere. If viscosity varies rapidly, however, most of the lithosphere may be strong enough to resist instability, which would diminish density-driven upwelling flow and also preserve the viscosity heterogeneity necessary for driving SDU. Using a moderate temperature-dependence of viscosity (with an activation energy of $E_A = 200$ kJ/mol), Korenaga and Jordan (2002) developed models of convective instabilities within lithospheric cavities and steps in the absence of asthenospheric shear. They computed upwelling rates of about 10 cm/yr assuming an asthenospheric viscosity of 10^{18} Pa s, which is consistent with estimates obtained from boundary layer theory. Upwelling rates, however, scale inversely with asthenospheric viscosity, and thus should be only ~1 or 0.1 cm/yr for asthenospheric viscosities of 10^{19} or 10^{20} Pa s, and even smaller if the temperature dependence of viscosity is greater (e.g., Hirth and Kohlstedt (1996) found $E_A > 200$ kJ/mol).

On Earth, asthenospheric shear is at most about 15 cm/yr (e.g., in the eastern Pacific) and in most places, especially continental environments, the rate of shear will be generally closer to 5 cm/yr or smaller. Given that SDU rates are at most ~4% to ~10% of the asthenospheric shear rate (for cavities and steps, respectively), the SDU will only control sublithospheric upwelling if density-driven upwelling is slower than 0.2–0.6 cm/yr near cavities and slower than 0.5–1.5 cm/yr near steps. This requires an asthenospheric viscosity of more than about $1–5 \times 10^{19}$ Pa s and/or a very sharp lithosphere–asthenosphere boundary that prevents cold lithosphere from dripping into the asthenosphere. The long-term stability of cratonic roots argues for a highly viscous cratonic lithosphere (Lenardic and Moresi, 1999), and the detection of sharp discontinuities within, and at the base of, continental lithosphere (Rychert et al., 2005; Rychert and Shearer, 2009) suggests that compositional heterogeneity may at least partially stabilize the lithosphere's basal structure. Thus, our requirement of sharp and sustained lithospheric topography may be reasonable in some cases, and for regions where asthenospheric shear flow is of order 5–10 cm/yr or more, it may be possible for SDU to dominate upwelling within a lithospheric cavity or step.

4.2. Upwelling within low-viscosity pockets

We have shown that a "pocket" of fluid embedded within a shearing asthenosphere can generate upwelling at rates up to ~20% of the imposed asthenospheric shear rate if the pocket is of optimal size and at least 2 orders of magnitude less viscous than the surrounding asthenosphere. However, the thermal, melt, or volatile conditions that can generate a pocket with a sufficient viscosity drop will also decrease the density of that pocket, which will induce upwelling flow that may overwhelm SDU. We estimate above that the required factor of 100 viscosity drop can be produced by a temperature increase of 200 °C, the presence of ~4% melt (if an accompanying a grain-size reduction is present Kohlstedt

and Zimmerman, 1996), or hydration of olivine corresponding to $\sim 810 \pm 490$ H/10^6 Si (Hirth and Kohlstedt, 1996). Of these, the most straightforward estimate of density is for 200 °C excess temperature in the thermal pocket, which will induce a decrease of ~0.6% (assuming a thermal expansivity of 3×10^{-5} K^{-1}), or ~20 kg/m^3. Fractional melting has been shown to decrease peridotite density by ~0.06% per 1% melt (Schutt and Lesher, 2006), which would produce 0.24% density reduction for 4% melt, or 8 kg/m^3. This assumes that the low-density melt is not removed from the system (e.g., to produce volcanism), which would produce a net increase in density and would also increase the viscosity of the remaining solid (Karato, 1986). Hydration of solid olivine is accommodated by crystal defects that produce approximately 1 metal vacancy for every 2 H (Zhao et al., 2004), so 810 H/10^6 Si will add ~400 vacancies per 10^6 Si, decreasing density by ~0.04%, or only ~1.3 kg/m^3 (G. Hirth, personal communication). However, the additional hydrogen and the increased compressibility of the defective olivine should tend to increase the density, partially negating the decrease due to vacancy introduction. Thus, we roughly estimate that olivine hydration should decrease density by at most ~1 kg/m^3 in the absence of melting, which should not generate significant buoyant upwelling. Once the hydrated rock partially melts, however, water will tend to move into the melt (Karato, 1986), which will increase viscosity. Noting these potentially complicated interactions between temperature, melt, and hydration, we estimate that these viscosity-decreasing factors will decrease density by ~20, ~8, and 1 kg/m^3, respectively.

The decreased densities of the low-viscosity pocket will tend to cause that pocket to rise within the asthenosphere. However, we found that SDU was most efficiently excited if the pocket was located immediately beneath the lithosphere (that is, $D_{LV} = 0$), which means that the pocket as a whole cannot continue to rise within the asthenosphere. Instead, a buoyant pocket will spread beneath the lithosphere as a gravity current, the fluid dynamics of which were discussed by Huppert (1982), and adapted for sub-lithospheric flows (especially plumes) by Bercovici and Lin (1996). In particular, Bercovici & Lin (1996, Fig. 1) showed that a compositionally buoyant disc of fluid that is about 10^3 times less viscous than its surroundings will thin by about 20% in a dimensionless time of about 7.2. To dimensionalize this quantity, we multiply by $H_0^2/12\kappa$, where $\kappa = 10^{-6}$ m^2/s is the thermal diffusivity and $H_0 = (80\kappa\eta_{LV}V_0/\Delta\rho g)^{1/6}$ is a dimensionless length scale (adapted here from Eq. (16) of Bercovici and Lin, 1996). Assuming a pocket viscosity of $\eta_{LV} = 10^{17}$ Pa s, a pocket volume of $V_0 = \pi(W_{LV}/2)^2 H_{LV} = \pi(500\,\text{km}/2)^2(80\,\text{km})$, and a density contrast of $\Delta\rho = 20$ kg/m^3 for a thermal anomaly, we obtain a dimensionless time of 2.3 Myr. Thinning a pocket of initial thickness $H_{LV} = 80$ km by 16 km (20%) in 7.2 dimensionless time units (16.6 Myr) causes the pocket base to move upward at only 0.1 cm/yr. Density contrasts consistent with melt or hydration of the pocket correspond to even slower upward rates of 0.07 and 0.04 cm/yr, respectively. By comparison, we found that upwelling rates of ~20% of the imposed asthenospheric shear rate are produced by SDU (for a viscosity contrast of 100 (Fig. 9), and presumably are even larger for the viscosity contrast of 1000 considered by Bercovici and Lin, 1996). Thus, even an asthenosphere shearing at a rate of only 1 cm/yr should produce a faster SDU (0.2 cm/yr) than is produced by the fastest gravity current (0.1 cm/yr) that would accompany the presence of the thermal pocket. SDU within melt or hydration pockets will be faster than gravity currents even if shear is only 0.7 and 0.4 cm/yr, respectively.

Thus, gravitational spreading of a low-viscosity and buoyant "pocket" beneath the lithospheric base should produce vertical rise rates that are slow compared to rates of induced SDU. This is because the gravity current produces primarily horizontal motion beneath the lithospheric base, which is slowed significantly in the case of a large viscosity contrast (Bercovici and Lin, 1996). More significant density-driven vertical motions may be associated with lithospheric "drips" into the low-viscosity pocket from above (e.g., Korenaga and Jordan, 2002), as described above for flow within lithospheric cavities and steps.

4.3. Surface volcanism produced by shear-driven upwelling

Upwelling flow will lead to decompression melting and melting instabilities if mantle rocks are already at their solidus (e.g., Raddick et al., 2002; Hernlund et al., 2008a,b). If asthenosphere is slightly below its solidus, then decompression melting can still occur if upwelling brings anomalously hot material upward from depth (e.g., Raddick et al., 2002) faster than thermal diffusion can equilibrate this material with its cooler surroundings. Although the height H_{up} that a hot fluid parcel must rise before it melts depends on the solidus and the parcel's initial depth and anomalous temperature, for SDU this rise height cannot be larger than the upwelling column (i.e., H_{up} is smaller than H_C or H_{LV}). Thus, an upper limit on the timescale for upwelling can be approximated as H_{up}/V_{up}, where V_{up} is the rise velocity. This timescale must be shorter than the timescale for lateral diffusion of this anomalously hot mantle, which we can approximate as W_{up}^2/κ where $\kappa = 10^{-6}$ m^2/s is the thermal diffusivity and W_{up} is the width of the upwelling. Thus, for a subsolidus asthenosphere, SDU can induce melting if (1) a sufficiently hot parcel is present at the SDU base and (2) upwelling is faster than $V_{up} > \kappa H_{up}/W_{up}^2$. We found above that $H_C \sim 100$ km excites SDU for typical cavities and steps, and $H_{LV} \sim 100$ km for SDU in asthenospheric pockets (~50% of H_{asth}). For cavity flow (Fig. 3a), the upwelling portion conservatively occupies ~25% of the cavity width, or $W_{up} \sim 50$ km if the cavity is 200 km wide. Upwelling in asthenospheric pockets occupies about 10% of the pocket width (Fig. 7b), or also $W_{up} \sim 50$ km for a 500 km wide pocket. Using these values, we roughly estimate that SDU of hot mantle must be faster than at most $V_{up} \sim 0.1$ cm/yr for melting to occur in an otherwise sub-solidus asthenosphere. Smaller minimum values of V_{up} are permitted for high anomalous temperature of a parcel or if the ambient mantle temperature is near the solidus, because these factor decrease H_{up} (e.g., $H_{up} \sim 0$ and $V_{up} \sim 0$ if the asthenosphere is at its solidus). Nevertheless, our upper bound estimate of $V_{up} \sim 0.1$ cm/yr is slower than rates we estimated above for SDU in optimally sized cavities (0.2 cm/yr), steps (0.5 cm/yr), and pockets (1.0 cm/yr) that are shearing at 5 cm/yr. Therefore, we should expect SDU to induce melting even if it is bringing heated mantle into a sub-solidus asthenosphere. Below we estimate rates of melting and surface volcanism assuming, as others have done (Raddick et al., 2002; Bianco et al., 2005; Hernlund et al., 2008a,b; Ballmer et al., 2007), that the asthenosphere is already very close to its solidus. However, for asthenosphere that is cooler than the solidus, it should be remembered that some component of upwelling will be devoted to elevating temperatures to the solidus before melting can occur, which will diminish total rates of melting and volcanism.

Assuming a near-solidus asthenosphere, we can estimate the rate of volcanism associated with SDU by first estimating the volume of melt that is produced by decompression melting. The fractional melting, f, produced by upwelling can be estimated by assuming vertical gradients for the solidus and adiabat, as well as melting parameters such as the latent heat of fusion and the specific heat (e.g., Phipps Morgan, 2001). Using estimates for these quantities, Raddick et al. (2002) estimated an adiabatic melt production of $df/dz = 0.27\%$ per km of upwelling. The melting behavior of upwelling mantle is actually more complicated and depends on the melting history and initial peridotite composition (e.g., Asimow et al., 1997; Phipps Morgan, 2001). For example, although olivine hydration may decrease the viscosity of the asthenosphere, and consequently induce SDU in a low-viscosity pocket, the increased

water content also tends to lower df/dz while increasing the depth at which peridotite crosses its solidus (e.g., Hirschmann et al., 1999). It is also important to consider the depth and thickness of the depleted layer (or residual mantle column), which may depend on conditions during previous melting episodes (e.g., Langmuir et al., 1992), relative to the depth at which upwelling occurs. If upwelling is focused in an already-depleted region of the mantle column, the total rate of melt production will be decreased. For example, mid-ocean ridge melting results in depletion that decreases with depth beneath oceanic lithosphere, whereas continental sub-lithosphere may have more complicated depletion profiles. Note that we do not expect pocket or cavity fluid to pass through a region of SDU more than once because recirculation times are typically longer than the expected lifetime of the driving shear flow (e.g., a complete circuit of a 500 km wide pocket at 1 cm/yr would require more than 100 Myr). A full study of melt production by SDU would simultaneously consider a range of mantle potential temperatures, peridotite equilibrium conditions, mantle dynamics and residual mantle columns (e.g., Langmuir et al., 1992; Ito and Mahoney, 2005). We leave such a treatment for future work, but here provide a first-order estimate of SDU melt production using Raddick et al.'s (2002) simple expression. In doing so, we assume, as others have, that decompression of the residual mantle column can reinitiate melting of the depleted layer (e.g., Bianco et al., 2005; Hernlund et al., 2008a,b; Ballmer et al., 2007).

By integrating the product of the adiabatic melt production (df/dz) and the upwelling rate through the thickness of the melting region, we can estimate the total rate of melt production (M) for a given column of rising asthenosphere. Although we have measured the maximum rate of upwelling, V_{max}, for SDU generated by lithospheric topography (Figs. 4 and 5) and asthenospheric pockets (Fig. 8), it is clear from Figs. 3 and 7 that this maximum rate does not apply for the entire upwelling column. We assume for simplicity that the rate of upwelling varies linearly with depth between V_{max} occurring within the anomaly and diminishing to zero at its top and bottom. For constant df/dz, the melting rate is:

$$M = \frac{df}{dz}\frac{H}{2}V_{max} \quad (3)$$

where H is the thickness of the SDU-inducing viscosity heterogeneity, which is given by $H_C = H_{asth}(1 - T_C)/T_C$ for cavities using (1) and $H_{LV} = H_{asth}H'_{LV}$ for pockets using (2). Using estimates for the lithospheric cavity considered above (Section 2.3; $H_{asth} = 200$ km, $T_C = 0.67$, and $V_{max} = 0.2$ cm/yr which is 4% of 5 cm/yr imposed shear), and $df/dz = 0.27\%$/km, we obtain a melt production rate of $M = 0.32$ km/Myr (assuming mantle and crustal densities of 3300 kg/m^3 and 2800 km/m^3, respectively). This means that a layer of melt 0.32 km thick is produced every Myr above the upwelling region of the lithospheric cavity. A lithospheric step (Section 2.3; $H_{asth} = 200$ km, $T_C = 0.5$, and $V_{max} = 0.5$ cm/yr which is 10% of 5 cm/yr imposed shear) should produce even faster rates of volcanism of $M = 0.80$ km/Myr. Finally, the fastest rates of SDU-induced volcanism are associated with a low-viscosity asthenospheric pocket (Section 3.4; $H_{asth} = 200$ km, $H'_{LV} = 0.4$, and $V_{max} = 1.0$ cm/yr which is 20% of 5 cm/yr imposed shear), for which we find $M = 2.5$ km/Myr. These estimates of upwelling assume that all of the melt that is produced in the upwelling column is erupted onto the surface. Although the eruption efficiency is uncertain and may be quite variable, it is thought that a large fraction of produced melts are erupted onto the surface (Trial et al., 1992). The above estimates of total melt production should probably be at least halved when converted into rates of surface eruption, giving a range of at most 0.16–1.3 km/Myr.

Basaltic oceanic crust averages ~7 km thick or more (e.g., White et al., 1992), suggesting that mid-ocean ridge volcanism produces significantly more melt than we expect from SDU, which is not surprising. Intraplate volcanism, however, can be significantly weaker and is potentially attributable to SDU. For example, at Crater Flat in Nevada, a region of basaltic volcanism in the Basin and Range Province, a minimum of approximately ~0.15–0.18 km^3 erupted in Pleistocene (Valentine et al., 2006), and more if additional basalt has been buried by alluvium. This volcanism may have been monogenetic, with each cone forming in a matter of years, but the total time span of volcanism was between 0.1 and 0.5 Myr (Valentine et al., 2006 and references therein). These estimates of volume and time span of volcanism suggest a rate of 0.3–1.8 km^3/Myr. The Crater Flat volcanism very roughly occurs over ~6–10 km^2, which includes gaps between the western-most cones. Assuming that the source area for volcanism is the same as the eruption area, we estimate a thickening rate of 0.03–0.3 km/Myr. As a point of reference, we estimate thickening rates of ~0.02–0.03 km/Myr for rejuvenation volcanism on some Hawaiian islands, which comprises <1% of the total volume of a given volcano (e.g., Walker, 1990; Swinnard et al., 2006). These minimum observed rates at Crater Flat are comparable to the lowest rates of volcanism that we have estimated for a simulation of SDU in a cavity, and are more than an order of magnitude smaller than estimates for a simulation with a low-viscosity pocket. Although these rate estimates for observed volcanism are rough, the fact that SDU-derived volcanism may be potentially more voluminous than observations of basaltic volcanism at an intraplate location like Crater Flat speaks to the potential significance of SDU for producing intraplate volcanism.

5. Discussion and conclusions

We have shown that localized shear-driven upwelling (SDU) can be generated in the asthenosphere by vigorous asthenospheric shear acting on large heterogeneities in asthenospheric or lithospheric viscosity. In particular, flow within a low-viscosity "cavity" embedded within the lithospheric base, as might be associated with a continental rift, can produce upwelling flow with magnitudes up to ~4% of the total velocity contrast across the asthenosphere. Flow near a step function change in lithospheric thickness, as might be associated with a cratonic edge, can produce upwelling at rates up to ~10% of the shear magnitude. In these cases, SDU is located against the cavity wall that faces the shear flow, but may be broadened or diminished if that wall is sloping. A second type of SDU can develop within a "pocket" of low-viscosity fluid, which can begin to circulate when exposed to asthenospheric shear. In this case, upwelling only occurs if the viscosity contrast is more than a factor of 10, the aspect ratio of the pocket is more than about 5, and the pocket occupies between ~20% and ~60% of the asthenospheric thickness. If the viscosity contrast is 100, then the upwelling arm of the pocket (located on the downstream side of the pocket) can produce SDU with a rate up to ~20% of the asthenospheric shear magnitude. Thus, if the total magnitude of shear across the asthenosphere is 5 cm/yr, viscosity heterogeneity associated with a lithospheric cavity, lithospheric step, or asthenospheric pocket can generate up to 0.2, 0.5, or 1.0 cm/yr of upwelling, respectively. This upwelling may decompress mantle peridotite, leading to melting. Depending on the thickness of the melting column and other petrological factors, SDU can generate sufficient upwelling in asthenospheric low-viscosity pockets and (to a lesser extent) lithospheric cavities to produce intraplate volcanism at the surface. Our first-order estimate is that SDU can produce 0.32–2.5 km/Myr of melt above a lithospehric cavity or low-viscosity pocket. If erupted to the surface, these values are comparable to, or larger than, estimates of continental volcanism rates at intraplate locations such as Crater Flat, Nevada.

Lateral variations in lithospheric viscosity may be associated with the lithosphere's thermal, chemical, and deformational

history. For the asthenosphere, viscosity heterogeneity may be associated with excess temperature, melt or hydration within a low-viscosity "pocket" of the asthenosphere, within which SDU can be excited. These factors that produce viscosity heterogeneity, however, are all also associated with changes in density, which may induce buoyancy-driven upwelling flow that competes with SDU. For example, convective "drips" falling into the asthenosphere from the dense overlying lithosphere may produce return upwelling flow that is comparable to, or even larger than, SDU (Korenaga and Jordan, 2002). The growth of this type of convective instability depends critically on the viscosity profile of the lithosphere: if cold, dense lithospheric rocks are sufficiently viscous, they cannot be easily removed by convective instability (Conrad and Molnar, 1999), and SDU should dominate upwelling. In the asthenosphere, SDU should generally dominate upwelling if low-viscosity heterogeneity of the right size and shape is present, because buoyancy-driven upwelling (e.g., associated with gravity currents, Bercovici and Lin, 1996) for these optimal shapes is expected to be slow. This is particularly the case if hydration of olivine causes the diminished viscosity, because density changes associated with hydration are expected to be small.

Low-viscosity pockets within the asthenosphere should evolve with time in the presence of asthenospheric shear and SDU. For example, Manga (1996) showed that low-viscosity regions of the mantle should deform rapidly, changing shape and elongating with time. In some cases, elongation may actually enhance SDU if it moves the aspect ratio of a low-viscosity pocket toward a more optimal value. However, eventually thinning will yield a pocket size that is unfavorable for SDU. In addition, shearing of a low-viscosity pocket should cause the pocket "walls" to slant, which may slow upwelling as the wedge-shaped corner of the pocket moves beneath higher viscosity asthenosphere. Simple shear deformation will cause an originally vertical pocket wall to slant by 45° (horizontal translation of the pocket base by a distance H_{LV}) in a time $\Delta t = V/H_{\mathrm{asth}}$. This timescale is about 4 Myr for a 200 km thick asthenosphere shearing at 5 cm/yr, although this timescale should not necessarily be interpreted as the expected lifetime of SDU because it is not yet clear exactly how slanting walls affect SDU. In addition, a pocket wall may not have been originally vertical, and removal of melt from the pocket may increase viscosity on the pocket edge, which could diminish or enhance wall slants depending on the depth of melting. Furthermore, Bercovici and Lin (1996) showed that gravity currents with large viscosity contrasts maintain steep sides at their edges, which suggests that any buoyancy associated with the low-viscosity pocket may help shearing pockets maintain vertical walls. Further study of the time-dependent evolution of SDU within deforming low-viscosity pockets, both with and without buoyancy effects and melting, will be needed to understand how we might expect SDU-induced volcanism to vary as a function of time.

Tomographic studies of the asthenosphere show a variety of shapes and sizes of low-velocity anomalies that presumably result from a variety of time-dependent processes. It is not immediately clear how SDU manifests itself for these non-rectangular shapes. In addition, the calculations presented here were performed in two dimensions, and thus are most relevant for geometries in which viscosity heterogeneity is elongated in the dimension perpendicular to the flow field. Regions like the western US, which features an east–west flow field (Silver and Holt, 2002; Conrad et al., 2007), north–south variations in lithospheric thickness (e.g., the cratonic edge or the lithospheric described by Zandt et al. (1995)), and potentially extensive asthenospheric heterogeneity (van der Lee and Frederiksen, 2005) might be adequately described in two dimensions. However, a viscosity heterogeneity that is limited in the flow-perpendicular dimension, or a flow field that is sub-perpendicular to the strike of lithospheric basal topography, may yield rates of SDU that are smaller than we have constrained here for two dimensions. As a result, further study is necessary to characterize the time-dependent behavior of SDU for a variety of geometries, and in three-dimensions. Additional seismological and geochemical constraints on the sizes, shapes, and viscosity contrasts associated with asthenospheric heterogeneity would significantly aid this effort.

Most previous studies that invoke sub-lithospheric processes to explain localized intraplate volcanism do so by creating upwelling via density heterogeneity: small-scale convection, return flow from lithospheric "drips", edge-driven convection, and even plume impingement, are all examples of how density heterogeneity, in these cases associated with convective processes, can induce upwelling flow. Here, we have shown that viscosity heterogeneity can alternatively drive upwelling flow if it occurs in the presence of vigorous asthenospheric shear. We note that upwelling flow can be induced even in the absence of any density heterogeneity or convective processes. Thus, the shear-driven upwellings (SDU) described here are fundamentally different than the upwellings associated with convective processes. Even Richter Rolls (e.g., Richter and Parsons, 1975; Korenaga and Jordan, 2003), which exist in the presence of a shear flow, rely on density heterogeneity and convection to maintain themselves. By contrast, SDU, which requires shear flow and viscosity heterogeneity only, may help explain numerous examples of intraplate volcanism that occur above rapidly shearing asthenosphere. One current example may be the basaltic volcanic fields of western North America (Wannamaker et al., 2001), where intraplate volcanism is difficult to explain via other processes (Smith et al., 2002; Smith and Keenan, 2005) and the underlying lithospheric and asthenospheric layers appear to be both shearing vigorously (Silver and Holt, 2002; Conrad et al., 2007) and laterally heterogeneous (Humphreys and Dueker, 1994; Zandt et al., 1995; Dueker et al., 2001; van der Lee and Frederiksen, 2005).

Acknowledgements

We thank editor Mark Jellinek, John Hernlund, an anonymous reviewer, and Mark Parmentier for comments that helped improve the manuscript, and the Nevada Agency for Nuclear Projects for support.

References

Anderson, D.L., 2000. The thermal state of the upper mantle: no role for mantle plumes. Geophys. Res. Lett. 27, 3623–3626.
Asimow, P.D., Hirschmann, M.M., Stolper, E.M., 1997. An analysis of variations in isentropic melt productivity. Philos. Trans. R. Soc. Lond. A 355, 255–281.
Ballmer, M.D., van Hunen, J., Ito, G., Tackley, P.J., Bianco, T.A., 2007. Non-hotspot volcano chains originating from small-scale sublithospheric convection. Geophys. Res. Lett. 34, L23310, doi:10.1029/2007GL031636.
Bercovici, D., Lin, J., 1996. A gravity current model of cooling mantle plume heads with temperature-dependent buoyancy and viscosity. J. Geophys. Res. 101, 3291–3309.
Bianco, T.A., Ito, G., Becker, J., Garcia, M., 2005. Secondary Hawaiian volcanism formed by flexural arch decompression. Geochem. Geophys. Geosys. 6, doi:10.1029/2005GC000945.
Bradshaw, T.K., Hawkesworth, C.J., Gallagher, K., 1993. Basaltic volcanism in the southern Basin and Range: no role for a mantle plume. Earth Planet. Sci. Lett. 116, 45–62.
Conrad, C.P., 2000. Convective instability of thickening mantle lithosphere. Geophys. J. Int. 143, 52–70.
Conrad, C.P., Molnar, P., 1999. Convective instability of a boundary layer with temperature- and strain-rate-dependent viscosity in terms of 'available buoyancy'. Geophys. J. Int. 139, 51–68.
Conrad, C.P., Behn, M.D., Silver, P.G., 2007. Global mantle flow and the development of seismic anisotropy: Differences between the oceanic and continental upper mantle. J. Geophys. Res. 112, B07317, doi:10.1029/2006JB004608.
Courtillot, V., Davaille, A., Besse, J., Stock, J., 2003. Three distinct types of hotspots in the Earth's mantle. Earth Planet. Sci. Lett. 205, 295–308.
Clouard, V., Bonneville, A., 2001. How many Pacific hostpots are fed by deep-mantle plumes? Geology 29, 695–698.

Dueker, K., Yuan, H., Zurek, B., 2001. Thick-structured Proterozoic lithosphere of the Rocky Mountain Region. GSA Today 11 (12), 4–9.
Foulger, G.R., Natland, J.H., 2003. Is "hotspot" volcanism a consequence of plate *tectonics?* Science 300, 921–922.
Gaherty, J.B., Kato, M., Jordan, T.H., 1999. Seismological structure of the upper mantle: a regional comparison of seismic layering. Phys. Earth Planet. Int. 110, 21–41.
Gürcan, F., 2005. Streamline topologies near a stationary wall of Stokes flow in a cavity. Appl. Math. Comput. 165, 329–345.
Hawkesworth, C., Turner, S., Gallagher, K., Bradshaw, T., Rogers, N., 1995. Calc-alkaline magmatism, lithospheric thinning, and extension in the Basin and Range. J. Geophys. Res. 100, 10271–10286.
Haxby, W.F., Weissel, J.K., 1986. Evidence for small-scale mantle convection from Seasat altimeter data. J. Geophys. Res. 91, 3507–3520.
Hernlund, J.W., Stevenson, D.J., Tackley, P.J., 2008a. Buoyant melting instabilities beneath extending lithosphere: 2. Linear analysis. J. Geophys. Res. 113, doi:10.1029/2006JB004863.
Hernlund, J.W., Tackley, P.J., Stevenson, D.J., 2008b. Buoyant melting instabilities beneath extending lithosphere: 1. Numerical models. J. Geophys. Res. 113, doi:10.1029/2006JB004862.
Hillier, J.K., Watts, A.B., 2007. Global distribution of seamounts from ship-track bathymetry data. Geophys. Res. Lett. 34, L13304, doi:10.1029/2007GL029874.
Hirschmann, M.M., Asimow, P., Ghiorso, M., Stolper, E., 1999. Calculation of peridotite partial melting from thermodynamic models of minerals and melts III: Controls on isobaric melt production and the effect of water on melt production. J. Petrol. 40, 831–851.
Hirth, G., Kohlstedt, D.L., 1995a. Experimental constraints on the dynamics of partially molten upper mantle: Deformation in the diffusion creep regime. J. Geophys. Res. 100, 1981–2001.
Hirth, G., Kohlstedt, D.L., 1995b. Experimental constraints on the dynamics of partially molten upper mantle 2. Deformation in the dislocation creep regime. J. Geophys. Res. 100, 15441–15449.
Hirth, G., Kohlstedt, D.L., 1996. Water in the oceanic upper mantle: implications for rheology, melt extraction and the evolution of the lithosphere. Earth Planet. Sci. Lett. 144, 93–108.
Humphreys, E.D., Dueker, K.G., 1994. Western U.S. upper mantle structure. J. Geophys. Res. 99, 9615–9634.
Huppert, H.E., 1982. The propagation of two-dimensional and axisymmetric viscous gravity currents over a rigid horizontal surface. J. Fluid Mech. 121, 43–58.
Ito, G., Mahoney, J., 2005. Flow and melting of a heterogeneous mantle: 1. Method and importance to the geochemistry of ocean island and mid-ocean ridge basalts. Earth Planet. Sci. Lett. 230, 29–46.
Jaupart, C., Mareschal, J.C., 1999. The thermal structure and thickness of continental roots. Lithos 48, 93–114.
Karato, S., 1986. Does partial melting reduce the strength of the upper mantle? Nature 319, 309–310.
Karato, S.-i., Jung, H., 1998. Water, partial melting and the origin of the seismic low velocity and high attenuation zone in the upper mantle. Earth Planet. Sci. Lett. 157, 193–207.
King, S.D., Raefsky, A., Hager, B.H., 1990. ConMan: vectorizing a finite element code for incompressible two-dimensional convection in the Earth's mantle. Phys. Earth Planet. Int. 59, 195–207.
King, S.D., Anderson, D.L., 1998. Edge-driven convection. Earth Planet. Sci. Lett. 160, 289–296.
King, S.D., Hager, B.H., 1990. The relationship between plate velocity and trench viscosity in Newtonian and power-law subduction calculations. Geophys. Res. Lett. 17, 2409–2412.
King, S.D., Ritsema, J., 2000. African hot spot volcanism: Small-scale convection in the upper mantle beneath cratons. Science 290, 1137–1140.
Kohlstedt, D.L., Evans, B., Mackwell, S.J., 1995. Strength of the lithosphere: constraints imposed by laboratory experiments. J. Geophys. Res. 100, 17587–17602.
Kohlstedt, D.L., Zimmerman, M.E., 1996. Rheology of partially molten mantle rocks. Annu. Rev. Earth Planet Sci. 24, 41–62.
Korenaga, J., Jordan, T.H., 2002. On the state of sublithospheric upper mantle beneath a supercontinent. Geophys. J. Int. 149, 179–189.
Korenaga, J., Jordan, T.H., 2003. Linear stability analysis of Richter rolls. Geophys. Res. Lett. 30, 2157, doi:10.1029/2003GL018337.
Langmuir, C., Klein, E., Plank, T., 1992. Petrological systematics of mid-ocean ridge basalts: constraints on melt generation beneath ocean ridges. In: Phipps Morgan, J., Blackman, D., Sinton, J. (Eds.), Mantle Flow and Melt Generation at Mid-Ocean Ridges. Geophysical Monograph, vol. 71. American Geophysics Union, pp. 183–280.
Le Pourhiet, L., Gurnis, M., Saleeby, J., 2006. Mantle instability beneath the Sierra Nevada mountains in California and Death Valley extension. Earth Planet. Sci. Lett. 25, 104–119.
Lei, J., Zhao, D., 2005. P-wae tomography and origin of the Changbai intraplate volcano in Northeast Asia. Tectonophysics 397, 281–295.
Lenardic, A., Moresi, L.-N., 1999. Some thoughts on the stability of cratonic lithosphere: Effects of buoyancy and viscosity. J. Geophys. Res. 104, 12747–12758.
Manga, M., 1996. Mixing of heterogeneities in the mantle: Effect of viscosity differences. Geophys. Res. Lett. 23, 403–406.
McKenzie, D., Bickle, M.J., 1988. The volume and composition of melt generated by extension of the lithosphere. J. Petrol. 29, 625–679.
Morgan, W.J., 1971. Convection plumes in the lower mantle. Nature 230, 42–43.
Moschetti, M.P., Ritzwoller, M.H., Shapiro, N.M., 2007. Surface wave tomography of the western United States from ambient seismic noise: Rayleigh wave group velocity maps. Geochem. Geophys. Geosyst. 8, Q08010, doi:10.1029/2007GC001655.
Pakdel, P., Spiegelberg, S.H., McKinley, G.H., 1997. Cavity flows in Elastic liquids: Two-dimensional flows. Phys. Fluids 9, 3123–3140.
Parsons, T., Thompson, G.A., Sleep, N.H., 1994. Mantle plume influence of the Neogene uplift and extension of the U.S. western Cordillera? Geology 22, 83–86.
Phipps Morgan, J., 2001. Thermodynamics of pressure release melting of a veined plum pudding mantle. Geochem. Geophys. Geosyst. 2, 2000GC000049.
Raddick, M.J., Parmentier, E.M., Scheirer, D.S., 2002. Buoyant decompression melting: A possible mechanism for intraplate melting. J. Geophys. Res. 107 (B10), 2228, doi:10.1029/2001JB000617.
Richards, M.A., Duncan, R.A., Courtillot, V., 1989. Flood basalts and hot spot tracks: Plume heads and tails. Science 246, 103–107.
Richter, F.M., Parsons, B., 1975. On the interaction of two scales of convection in the mantle. J. Geophys. Res. 80, 2529–2541.
Rychert, C.A., Fischer, K.M., Rondenay, S., 2005. A sharp lithosphere-asthenosphere boundary imaged beneath eastern North America. Nature 436, 542–545.
Rychert, C.A., Shearer, P.M., 2009. A global view of the lithosphere-asthenosphere boundary. Science 324, 495–498.
Schmeling, H., 1985. Numerical models on the influence of partial melt on elastic, anelastic and electric properties of rocks. Part I: elasticity and anelasticity. Phys. Earth Planet. Int. 41, 34–57.
Schmeling, H., Bussod, G.Y., 1996. Variable viscosity convection and partial melting in the continental asthenosphere. J. Geophys. Res. 101, 5411–5423.
Schutt, D.L., Lesher, C.E., 2006. Effects of melt depletion on the density and seismic velocity of garnet and spinel lherzolite. J. Geophys. Res. 111, B05401, doi:10.1029/2003JB002950.
Shankar, P.N., Deshpande, M.D., 2000. Fluid mechanics in the driven cavity. Ann. Rev. Fluid Mech. 32, 93–136.
Shaw, J.E., Baker, J.A., Menzies, M.A., Thirlwall, M.F., Ibrahim, K.M., 2003. Petrogenesis of the largest intraplate volcanic field on the Arabian plate (Jordan): a mixed lithosphere-asthenosphere source activated by lithospheric extension. J. Petrol. 44, 1657–1679.
Shen, C., Floryan, J.M., 1985. Low Reynolds number flow over cavities. Phys. Fluids 28, 3191–3202.
Silver, P.G., Holt, W.E., 2002. The mantle flow beneath western North America. Science 295, 1054–1057.
Sleep, N.H., 1990. Hotspots and mantle plumes: some phenomenology. J. Geophys. Res. 95, 6715–6736.
Smith, E.I., Keenan, D.L., 2005. Yucca Mountain could face greater volcanic threat. EOS Trans. Am. Geophys. Union 86, 312–317.
Smith, E.I., Keenan, D.L., Plank, T., 2002. Episodic volcanism and hot mantle: Implications for volcanic hazard studies at the proposed nuclear waste repository at Yucca Mountain, Nevada. GSA Today 12, 4–10.
Stein, C.A., Stein, S., 1992. A model for the global variation in oceanic depth and heat flow with lithospheric age. Nature 359, 123–129.
Steinberger, B., 2000. Plumes in a convecting mantle: Models and observations for individual hotspots. J. Geophys. Res. 105, 11127–11152.
Swinnard, L., Gandy, C., Garcia, M.O., Weis, D., 2006. Evaluation of source components and processes forming the Koloa Volcanics, of Kauai, Hawaii, based on Pb, Sr, and Nd isotopic evidence. EOS Trans. AGU 87 (52 (Fall Meet. Suppl.)) (Abstract V13B-0689).
Toomey, D.R., Wilcock, W.S.D., Solomon, S.C., Hammond, W.C., Orcutt, J.A., 1998. Mantle seismic structure beneath the MELT region of the East Pacific Rise from P and S wave tomography. Science 280, 1224–1227.
Trial, A.F., Spera, F.J., Greer, J., Yuen, D.A., 1992. Simulations of magma withdrawal from compositionally zoned bodies. J. Geophys. Res. 97, 6713–6733.
Valentine, G.A., Perry, F.V., Krier, D., Keating, G.N., Kelley, R.E., Cogbill, A.H., 2006. Small volume basaltic volcanoes: eruptive products and processes, and posteruptive geomorphic evolution in Crater Flat (Pleistocene), southern Nevada. GSA Bull. 118, 1313–1330.
van der Lee, S., Frederiksen, A., 2005. Surface wave tomography applied to the North America Upper Mantle. In: Nolet, G., Levander, A. (Eds.), Seismic Earth: Array Analysis of Broadband Seismograms. Geophysical Monograph Series, 157, 67–80.
van Hunen, J., Zhong, S., 2006. Influence of rheology on realignment of mantle convective structure with plate motion after a plate reorganization. Geochem. Geophys. Geosyst. 7, Q08008, doi:10.1029/2005GC001209.
van Wijk, J., van Hunen, J., Goes, S., 2008. Small-scale convection during continental rifting: Evidence from the Rio Grande rift. Geology 36, 575–578.
Walker, G.P.L., 1990. Geology and volcanology of the Hawaiian Islands. Pacific Sci. 44, 315–347.
Wang, K., Plank, T., Walker, J.D., Smith, E.I., 2002. A mantle melting profile across the Basin and Range, southwestern USA. J. Geophys. Res. 107, doi:10.1029/2001JB000209.
Wannamaker, P.E., Bartley, J.M., Sheehan, A.F., Jones, C.H., Lowry, A.R., Dimitru, T.A., Ehlers, T.A., Holbrook, W.S., Farmer, G.L., Unsworth, M.J., Hall, D.B., Chapman, D.S., Okaya, D.A., John, B.E., Wolfe, J.A., 2001. The Great Basin-Colorado Plateau transition in central Utah: an interface between active extension and stable interior. In: Erskine, M.C., Faulds, J.E., Bartley, J.M., Rowley P. (Eds.), The Geological Transition: Colorado Plateau to Basin and Range. UGA/AAPG Guideb. 30/GB78, pp. 1–38.
Wessel, P., 1997. Sizes and ages of seamounts using remote sensing: Implications for intraplate volcanism. Science 277, 802–805.

West, M., Ni, J., Baldridge, W.S., Wilson, D., Aster, R., Gao, W., Grand, S., 2004. Crust and upper mantle shear wave structure of the southwest United States: Implications for rifting and support for high elevation. J. Geophys. Res. 109, B03309, doi:10.1029/2003JB002575.

White, R.S., McKenzie, D., O'Nions, R.K., 1992. Oceanic crustal thickness from seismic measurements and rare earth element inversions. J. Geophys. Res. 97, 19683–19715.

Zandt, G., Myers, S.C., Wallace, T.C., 1995. Crust and mantle structure across the Basin and Range–Colorado Plateau boundary at 37°N latitude and implications for Cenozoic extensional mechanism. J. Geophys. Res. 100, 10529–10548.

Zhao, H.-Y., Ginsberg, S.B., Kohlstedt, D.L., 2004. Solubility of hydrogen in olivine: dependence on temperature and iron content. Contrib. Mineral. Petrol. 147, 155–161.